Sub-micron elastic properties measurement of *single* laser-affected volume in fused silica

Yves Gaillard

Université de Franche-Comté, CNRS, FEMTO-ST Institute,
24 rue de l'épitaphe, F-25030 Besançon, France

Arunkrishnan Radhakrishnan, Yves Bellouard[+]

Ecole Polytechnique Fédérale de Lausanne (EPFL), Galatea Lab, Rue de la Maladière 71, CH-2002 Neuchâtel, Switzerland

Fabien Amiot[*]

Université de Franche-Comté, CNRS, FEMTO-ST Institute,
24 rue de l'épitaphe, F-25030 Besançon, France
[*]*fabien.amiot@femto-st.fr* , [+]*yves.bellouard@epfl.ch*

Abstract

Non-ablative femtosecond laser exposure of transparent substrates leads to bulk volumetric changes, and consequently, localised structural changes resulting in micron-scale variation of elastic properties in the material. Here, we demonstrate the use of grid nano-indentation to characterize the elastic stiffness field across the laser-modified volume. Sub-micron spatial resolution is achieved by adapting a deconvolution procedure to the laser-affected zone (LAZ) geometry that minimizes a projection residual out of which an elastic description of the modified glass is sequentially constructed. Thanks to this method, a bimodal stiffness-distribution across the laser-affected zones is revealed, highlighting the complex nature of the interaction.

Keywords:

Glass, nanoindentation, ultrafast laser processing, elastic behavior, Silica glass

1. Introduction

Femtosecond laser exposure of glass in the non-ablative regime can lead to various structural modifications, depending on laser parameters, such as pulse duration, pulse energy and exposure dose. In fused silica, it leads to various changes such as a localized densification [1], so called type I, the formation of self-organized nanostructures [2, 3] (type II) or nanoporous assembly [4] (ref. as type 'X'). These structural modifications induce localized volumetric changes [5, 6], and consequently the formation of a stress field. These modifications occur within the direct-exposed volume, which depending on the confocal parameters and because of the non-linear nature of the laser-matter interaction, can be of the characteristic size of the laser spot or smaller. Consequently, measuring them is particularly challenging, in particular when it comes to resolve elastic properties changes occurring within a few microns.

So far, photoelasticity [7], indirect methods making use of mechanical amplification like bimorph cantilevers [5, 8, 9], or larger volume made nanoindentation of several adjacent laser-modified zones [7] were used to estimate the elastic properties of laser-modified zones. While these methods provide a means for evaluating the average stress and volume expansion in laser-affected zones, it does not elucidate subtle variations of elastic properties *within* a laser-affected volume. For instance, at relatively high irradiance level [10, 11], it has been suspected that laser-affected zones may have bi-modal structures, consisting in self-organized nanostructures along the propagation front and densified zones at the tail. However, these observations remain speculative, due to a lack of accurate method to resolve these fine variations in density and consequently in the elastic modulus. Beyond the pure scientific interest, acquiring additional information about the fine mechanical behavior at the nanoscale level along laser affected zones also has important implications for practical applications, in particular for elucidating the long-term strain behavior of laser-affected zones [12, 13].

Here, we proposed to adapt a method based on grid nano-indentation [14] to resolve these fine features. This method contributes to a refined analysis of how the structure of materials evolves under strong fields exposure and in particular, how their elastic properties are locally modulated.

2. Material and methods

In the following experiment, we considered fused silica substrates (Corning 7980 0F, rich OH content, $25\times25\times1$ mm) that we exposed to femtosecond laser radiation (Amplitude, OPA 800 nm, emitting 50 fs pulses with a repetition rate of 120 kHz). Technically, line-patterns are written across the substrate length at a depth of approximately 80 μm, and a speed of 500 μm/s. The incident radiation is linearly polarised with the electrostatic field perpendicular to the writing direction. The laser is focused using a 0.4 NA laser-objective. For the case reported here, the pulse energy is 300 nJ. After exposure, the substrate is diamond wire cut and polished until an optical finish is achieved to reveal the laser-affected zones cross-section. Figure 1 shows the typical morphology of the LAZ as seen using a atomic-force microscope (PSIA XE-150 from Park instruments in contact mode, along with the location of the nanoindents).

A total of $N = 220$ indentation tests are performed (UNHT1, Anton Paar) at points P_n on 22×10 indentation grid covering a LAZ and some pristine glass. The grid step is nominally 1 μm. Denoting f the applied force on the indenter, each indentation is realised with a $f = 1$ mN maximum load at a constant strain rate ($\dot{f}/f = 0.05$). To ensure a continuous stiffness measurement during the entire loading part of the curve, a sinusoidal signal with a 5 Hz frequency is superimposed. The indentation modulus $E_{eq}(P_n)$ is extracted following the Oliver and Pharr method [15]. This stiffness is hereafter translated into the Young's modulus $M(P_n)$ of the equivalent uniform isotropic material, assuming that its Poisson's coefficient is $\nu = 0.17$ and considering $E_i = 1141$ GPa and $\nu_i = 0.07$ for the indenter material.

$$\frac{1}{E_{eq}(P_n)} = \frac{1-\nu_i^2}{E_i} + \frac{1-\nu^2}{M(P_n)} \tag{1}$$

The calibration of the shape of the indenter is performed indenting a material with a known Young's modulus and Poisson's ratio (fused silica). The projected contact area at maximum load $A_c(P_n) = \pi a_n^2$ is also obtained from this calibration, thus defining the equivalent contact radius a_n.

After indentation, the sample's topography was measured by atomic force microscopy and is displayed in Fig. 1. It is first used to manually locate the

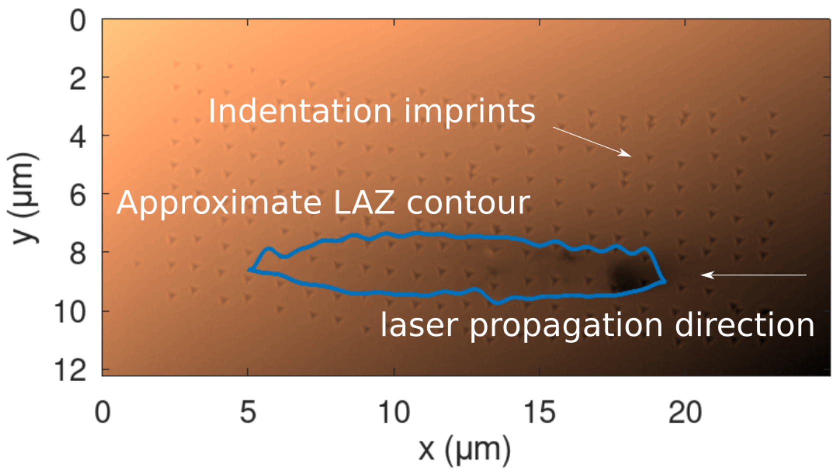

Figure 1: Topography of measurement area. The considered LAZ is highlighted with a blue line.

boundaries of the LAZ : the user hand picks the limits of the LAZ, and a subsequent interpolation allows to define its continuous closed contour. As the processing scanning direction is orthogonal to the plane of the of Fig. 1, the three-dimensional LAZ is assumed to be a semi-infinite cylinder $\mathcal{C}$ whose basis is the above-defined closed contour. The sample's topography is also used to precisely locate the indents with respect to the LAZ. This is crucial since positioning errors are unavoidable with the technology of the used nano-indentation system. The remaining error on the indent location is driven by the AFM image resolution, and is estimated to be about 25 nm, which is much smaller than the typical size of the residual imprint. A raw map of the measured indentation moduli is obtained assuming linear interpolation between the indents (see Fig. 2).

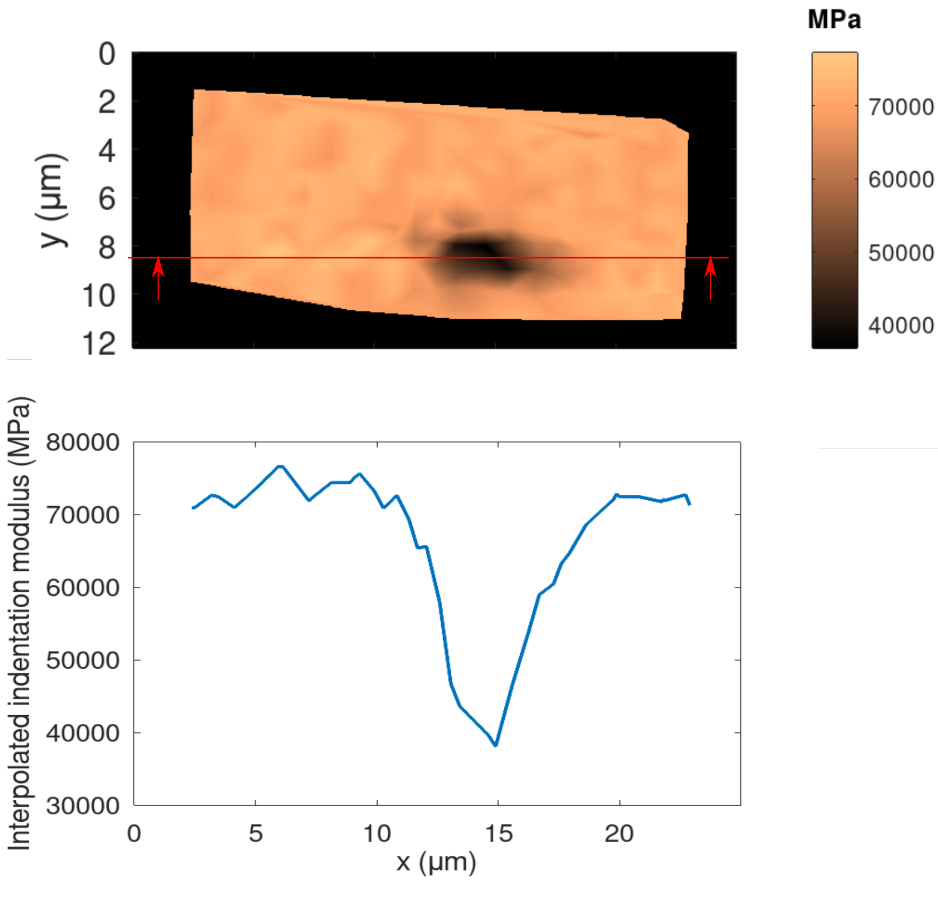

Figure 2: Measured indentation modulus map, assuming linear interpolation between the indents. The bottom graph displays a one-dimensional spatial modulus distribution along the laser beam propagation direction, as indicated by a red line in the modulus map.

3. Theory and calculation

The raw measurements in Fig. 2 actually result from the convolution of the actual indentation modulus map with a mechanical convolution kernel depending on the elastic fields under the indenter at the measurement force [14]. Because of the very fine details in the LAZ, this convolution significantly blurs the resulting picture, and it is necessary to deconvolve this map in order to retrieve a description of the elastic properties fields inside the LAZ. This deconvolution procedure relies on an a priori parametrized description of the elastic parameter field. One approach is to first assume that the LAZ displays a uniform elasticity, so that its stiffness M_{LAZ} and the stiffness of the surrounding glass matrix M_{glass} are the sole elastic parameters to retrieve from the N indentation measurements. The deconvolution relies on a scaled strain energy density $e(a, \nu, \rho, z)$ at a point (ρ, z) under the contact to define an influence coefficient at a given point P, $I(\nu, a, P, \mathcal{C})$ [14] expressed as:

$$I(\nu, a, P, \mathcal{C}) = \frac{\int_{\mathcal{C}} e(a, \nu, \rho, z)dV}{\int_{\mathcal{H}} e(a, \nu, \rho, z)dV} \tag{2}$$

where $\mathcal{H}$ and $\mathcal{C}$ stand for the full half-space and semi-infinite cylinder, respectively, and where ρ and z are the cylindrical coordinates.

$I(\nu, a, P, \mathcal{C})$ is independent from the probed elastic properties besides the Poisson's ratio, which is arbitrarily set to $\nu = 0.17$ for both material phases (i.e. pristine and laser-modified). The integral is calculated for z ranging from 0 to $10 \times a$ and for ρ ranging from 0 to $10 \times a$. These bounds are very large considering that e vanishes at a distance about a. This further suggests that the effect of the nearby indentation point is negligible. The theoretical indentation modulus at any point P, $M_{th}(P)$ reads:

$$M_{th}(P) = M_{LAZ} I(\nu, a, P, \mathcal{C}) + M_{glass}(1 - I(\nu, a, P, \mathcal{C})) \tag{3}$$

The same equation can be derived for any of the N measurement points P_n. Here, the influence coefficient $I(0.17, a_n, P_n, \mathcal{C})$ is almost never 1, meaning that the LAZ is never probed alone, but is influenced by the unmodified regions. Because of both modelling and measurement errors, the measured

$M(P_n)$ may deviate from $M_{th}(P_n)$. By combining all the equations (3) for all the measurement points N, one obtains an over-determined set of N linear equations depending on two unknowns, so that all the N equations cannot be satisfied simultaneously, in general. The system is thus solved in a least-square sense to provide the sought elastic parameters together with a projection residual $R(P_n)$ at a point P_n, expressed as:

$$R(P_n) = M_{LAZ} I(\nu, a_n, P_n, \mathcal{C}) + M_{glass}(1 - I(\nu, a_n, P_n, \mathcal{C})) - M(P_n) \quad (4)$$

The overall quality of the proposed description may also be appreciated using the average normalized residual η, defined as:

$$\eta = \sqrt{\frac{\sum_n R(P_n)^2}{\sum_n M(P_n)^2}} \quad (5)$$

4. Results and discussion

Applied to our measurements, we obtain $M_{LAZ} = 60.9$ GPa and $M_{glass} = 70.9$ GPa, for an average residual $\eta = 6.4 \times 10^{-2}$. This rather poor initial guess (which was to assume a uniform elastic distribution) is confirmed by the residual field displayed in Fig. 3, which clearly suggests that the LAZ is elastically significantly non-uniform. It should however be highlighted that the value M_{glass} obtained outside the LAZ perfectly fits the reference value for such glass. This proves that the sample preparation (cutting and polishing) did not significantly alter the mechanical properties of the material.

To improve the elastic distribution hypothesis of the LAZ, we now consider a bimodal distribution. This is equivalent to divide the LAZ into two uniform zones separated by a boundary located at a position $x = x_b$. The

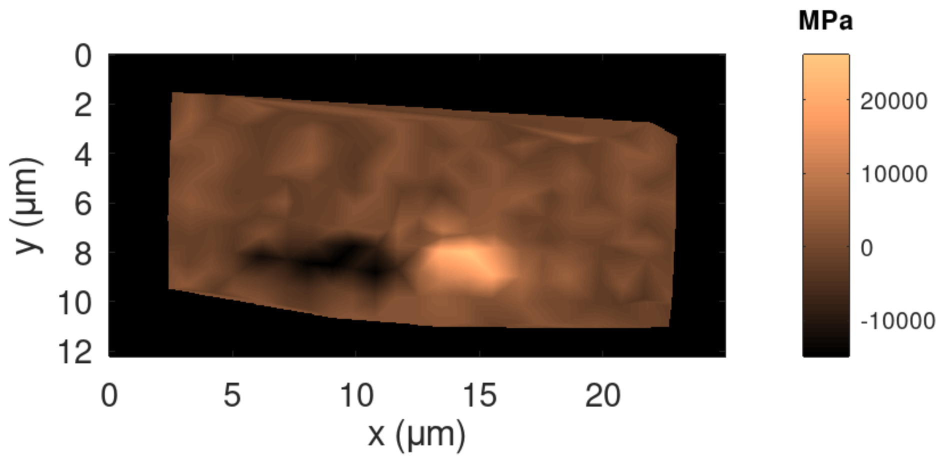

Figure 3: Projection residual map $R(P_n)$ assuming a uniform LAZ and linear interpolation between the indents. Two distinct zones are revealed, highlighting the inaccuracy of the initial guess estimate of the elastic distribution. The residual map also suggests the existence of a bi-modal elastic properties distribution.

theoretical indentation modulus at point P, $M_{th}(P)$ now reads:

$$\begin{aligned} M_{th}(P) \quad &= \quad M_{LAZ,left} I_{left}(\nu, a, P, \mathcal{C}, x_b) + M_{LAZ,right} I_{right}(\nu, a, P, \mathcal{C}, x_b) \\ &\quad + M_{glass}(1 - I_{left}(\nu, a, P, \mathcal{C}, x_b) - I_{right}(\nu, a, P, \mathcal{C}, x_b)) \qquad (6) \end{aligned}$$

and the deconvolution procedure is repeated for any position x_b across the boundary.

Fig. 4 displays the overall indicator η as a function of the position x_b of the boundary chosen to divide the LAZ into two distinct zones. A clear minimum is found at $x_b = 12.4\ \mu m$ with $\eta(x_b = 12.4\ \mu\text{m})$=4.7 $\times 10^{-2}$, thus demonstrating a clear improvement compared to the initial description (compared to the initial residual value of 6.4×10^{-2}). For this optimized description, the identified elastic parameters are $M_{LAZ,left} = 73.0$ GPa, $M_{LAZ,right} = 52.4$ GPa

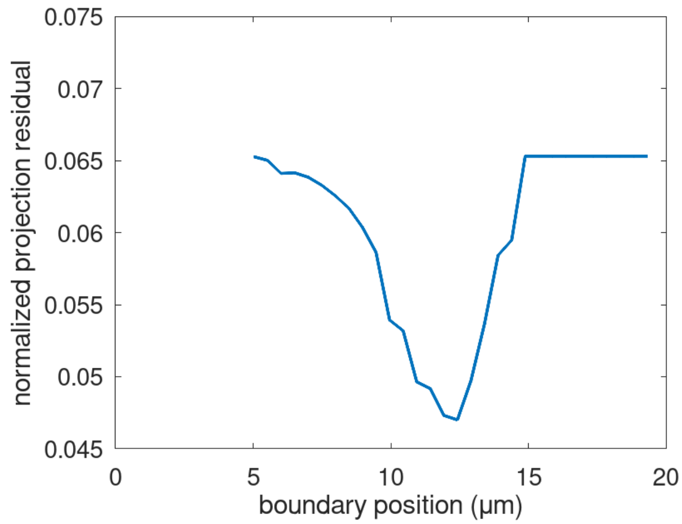

Figure 4: Global projection residual η of the boundary between the two sub-LAZ as a function of the boundary position x_b.

and $M_{glass} = 70.8$ GPa.

The corresponding residual map is displayed in Fig.5. Both the amplitude of the residual distribution and its spatial distribution have been significantly reduced, thereby indicating that a bimodal elastic distribution described more accurately the actual elastic stiffness field after laser exposure.

The results show that, along the propagation axis, the material has first experienced a significant damage, resulting in a reduced stiffness. This is very consistent with a reduced material density and with the porous nature of the nanogratings [3]. The obtained stiffness values suggest that a porosity of about $\simeq 30\%$ has been introduced in this degraded zone. The opposite behavior is then observed. The zone, where some self-focusing tends to be

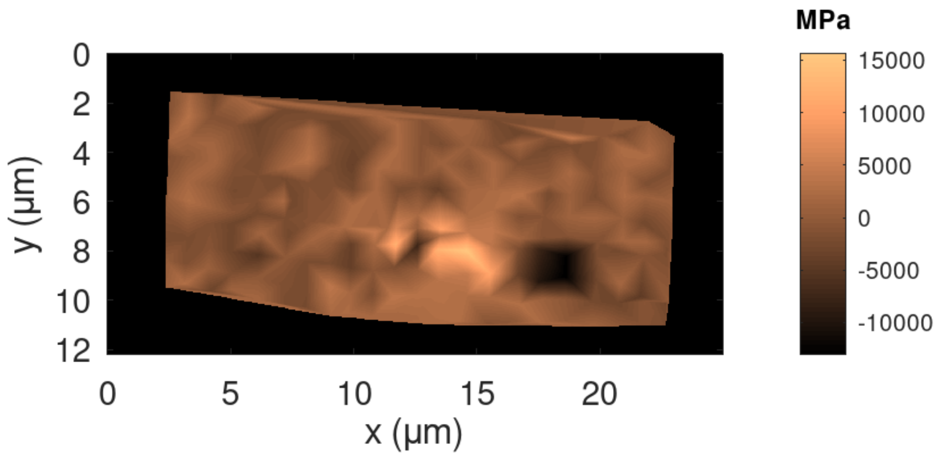

Figure 5: Projection residual map $R(P)$ assuming a bi-modal distribution of elasticity and considering a linear interpolation between the indents.

observed at higher energy displays a slightly higher stiffness. Interpreting this stiffness change as a density change suggests a glass compaction about $\simeq 3\%$ in this zone. This information shows that at high pulse energy, nanogratings have a complex mechanical behavior, combining *both* densified and porous zones. This more complex loading case may lead to additional shear strain at the interface, prone to crack nucleation that may weaken laser-modified zones and in turn devices. it defines an upper limit above which the mechanical integrity of direct-write structure can be compromised.

5. Conclusion

Combining grid nano-indentation technique with a dedicated deconvolution approach, we reveal the detail of the stiffness field inside a unique laser-affected volume in fused silica. To the best of our knowledge, this is the first time such spatially resolved information is obtained. This is thought to be of crucial importance in understanding the mechanisms involved in the glass modification induced by a non-ablative femtosecond laser exposure. This information shows that at high pulse energy, nanogratings have a complex mechanical behavior, combining *both* densified and porous zones. This outlines the capability of such fabrication technique to process graded materials with very steep stiffness gradients in the 10 GPa.μm^{-1} range.

Acknowledgements

This work benefited from the support of the collegium SMYLE. For the purpose of Open Access, a CC-BY public copyright licence has been applied by the authors to the present document and will be applied to all subsequent versions up to the Author Accepted Manuscript arising from this submission.

Authors contributions

YG performed the nanoindentation and AFM measurements, AR prepared the laser-exposed specimens, YG, FA, and YB performed the data analysis, FA and YB conceived the study, all authors contributed to the manuscript writing and revisions. The authors have no conflicts to disclose.

References

[1] K. Miura, J. Qiu, H. Inouye, T. Mitsuyu, and K. Hirao, "Photowritten optical waveguides in various glasses with ultrashort pulse laser," Applied Physics Letters 71 (1997) 3329–3331.

[2] Y. Shimotsuma, P. G. Kazansky, J. Qiu, and K. Hirao, "Self-Organized Nanogratings in Glass Irradiated by Ultrashort Light Pulses," Phys. Rev. Lett. 91 (2003), 247405.

[3] M. Lancry, B. Poumellec, J. Canning, K. Cook, J.-C. Poulin, and F. Brisset, "Ultrafast nanoporous silica formation driven by femtosecond laser irradiation: In the heart of nanogratings," Laser Photonics Reviews (2013), 1-10.

[4] M. Sakakura, Y. Lei, L. Wang, Y.-H. Yu, and P. G. Kazansky, "Ultralow-loss geometric phase and polarization shaping by ultrafast laser writing in silica glass," Light: Science Applications (2020), 9.

[5] A. Champion and Y. Bellouard, "Direct volume variation measurements in fused silica specimens exposed to femtosecond laser," Opt. Mater. Express 2 (2012), 789–798.

[6] Y. Bellouard, A. Champion, B. McMillen, S. Mukherjee, R. R. Thomson, C. Pépin, P. Gillet, and Y. Cheng, "Stress-state manipulation in fused silica via femtosecond laser irradiation," Optica 3 (2016), 1285.

[7] Y. Bellouard, T. Colomb, C. Depeursinge, M. Dugan, A. A. Said, and P. Bado, "Nanoindentation and birefringence measurements on fused silica specimen exposed to low-energy femtosecond pulses," Opt. Express 14 (2006), 8360–8366.

[8] P. Vlugter, E. Block, and Y. Bellouard, "Local tuning of fused silica thermal expansion coefficient using femtosecond laser," Physical Review Materials 3 (2019), 053802.

[9] P. Vlugter and Y. Bellouard, "Abnormal temperature dependent elastic properties of fused silica irradiated by ultrafast lasers," Phys. Rev. Materials 6 (2022), 033602.

[10] C. Hnatovsky, R. S. Taylor, P. P. Rajeev, E. Simova, V. R. Bhardwaj, D. M. Rayner, and P. B. Corkum, "Pulse duration dependence of femtosecond-laser-fabricated nanogratings in fused silica," Applied Physics Letters 87 (2005), 014104.

[11] B. McMillen, O. Uteza, R. Clady, N. Sanner, M. Sentis, F. Nabiei, Y. Cheng, and Y. Bellouard, "Laser-induced densification of fused silica using spatially overlapping sub-30 fs pulses," Journal of Applied Physics 128 (2020), 083107.

[12] S. I. Nazir, C. E. Athanasiou, and Y. Bellouard, "On the behavior of uniaxial static stress loaded micro-scale fused silica beams at room temperature," Journal of Non-Crystalline Solids: X 14 (2022), 100083.

[13] H. Yao, D. Pugliese, M. Lancry, and Y. Dai, "Ultrafast Laser Direct Writing Nanogratings and their Engineering in Transparent Materials," Laser & Photonics Reviews (2024), 2300891.

[14] Y. Gaillard and F. Amiot, Grid nano-indentation as full-field measurements, Composites Part A : applied science and manufacturing 132 (2020), 105807.

[15] W.C. Oliver and G.M. Pharr, Measurement of Hardness and Elastic Modulus by Instrumented Indentation: Advances in Understanding and Refinements to Methodology, J. Mater. Res 19 (2004) 3-20.